Walking-Induced Vibration of Steel-Framed Floors Supporting Sensitive Equipment

BRAD DAVIS and DI LIU

ABSTRACT

This paper explains the vibration evaluation methods for floors supporting sensitive equipment in the second edition of AISC Design Guide 11, *Vibrations of Steel-Framed Structural Systems Due to Human Activity*. It presents new experimentally verified equations that are simplified for practical implementation. Sensitive equipment tolerance limits are stated in numerous forms, including peak acceleration and various spectral acceleration and velocity. For this reason, response predictions are given in terms of all tolerance limit forms that are commonly used. The most severe responses of lower frequency floors to walking are due to resonant buildups, whereas the most severe responses of higher frequency floors are due to a series of individual footstep impulses; equations are given for both. Because the sensitive equipment tolerance limit is objective, each equation includes a calibration factor that results in a high probability that the predicted response will exceed the actual response.

Keywords: vibration, serviceability, floors, sensitive equipment.

INTRODUCTION

Steel-framed floors commonly support vibration-sensitive equipment in hospitals, laboratories, and other modern facilities. Sensitive equipment vibration tolerance limits are usually stringent, so walking vibration serviceability often requires much larger member sizes than those required for strength, deflection, or human comfort, even in quiet areas such as offices or residences. The consequence of objectionable vibration usually involves expensive and difficult retrofit solutions. The consequence of an overdesign is excessive steel tonnage. Thus, it is important that engineers have access to prediction methods that are accurate and have known levels of conservatism.

Until 2016, vibrations of floors supporting sensitive equipment had been evaluated using the American Institute of Steel Construction (AISC) Design Guide 11, *Floor Vibration Due to Human Activity* (Murray et al., 1997) Chapter 6, which is based on an approach suggested by Ungar and White (1979).

In recent years, updated response prediction methods have been developed (Young and Willford, 2001; Willford et al., 2007a, 2007b) and specialized by the writers for floors supporting sensitive equipment (Liu and Davis, 2015; Liu, 2015). These updated methods are the basis of Chapter 6 of the second edition of Design Guide 11 *Vibrations of Steel-Framed Structural Systems Due to Human Activity* (Murray et al., 2016). The purpose of this paper is to explain the methods and their design implementation.

The paper is organized into the following sections:

- Tolerance limits for vibration-sensitive equipment
- Prediction of modal properties
- Forces due to walking
- Prediction of resonant responses
- Prediction of impulse responses
- Response prediction
- Commentary on first and second editions of AISC Design Guide 11, Chapter 6
- Conclusions

TOLERANCE LIMITS FOR VIBRATION-SENSITIVE EQUIPMENT

Equipment manufacturers provide specific tolerance limits in terms of various vibration measures, for example, waveform peak acceleration, narrowband spectral acceleration, and one-third octave spectral velocity. An example of measured response to walking, showing the acceleration waveform, narrowband acceleration spectrum, and one-third octave velocity spectrum, is in Figure 1. Such specific limits should be used when possible.

Brad Davis, PhD, SE, Associate Professor, Department of Civil Engineering, University of Kentucky, Lexington, KY. Email: dbraddavis@uky.edu (corresponding)

Di Liu, Associate, Liftech Consultants Incorporated, Oakland, CA. Email: dliu@liftech.net

Paper No. 2018–13

Spectral limits can be converted from displacement to velocity or from velocity to acceleration by multiplying by $2\pi f$, where f is the frequency. For example, if the velocity limit at 8 Hz is 3000 μin./sec (mips), then the corresponding acceleration limit at 8 Hz is 0.151 in./sec^2 = 0.0391%g.

Most spectral limits are in terms of root-mean-square (RMS) accelerations or velocities, but occasionally they are in terms of peak quantities. A peak spectral limit is converted to RMS by multiplying by 0.7071. Often, the type of spectrum, peak versus RMS, is not clear; in such cases, the equipment manufacturer should be contacted.

If the type, but not model, of equipment has been identified, or if the manufacturer does not provide a specific limit, then generic tolerance limits should be used. The most common generic limits are the vibration criterion (VC) curves (Ungar et al., 2006) that are the basis of AISC Design Guide 11, Table 6-2, and are stated in terms of RMS velocity in one-third octave bands of frequency.

Tolerance limits for sensitive equipment are usually considered definitive. "Failure" of the floor vibration limit state for sensitive equipment is considered to correspond to equipment malfunction. Equipment manufacturers often require site surveys in which actual velocity levels are compared to the tolerance limit. When the measured values exceed the limit, difficult and expensive retrofit solutions are usually required. Thus, in the following sections, the objective is to predict the vibration magnitudes that will be measured by the site surveyor, and a calibration factor is included to ensure a low probability that the measured values will exceed the ones predicted during design.

PREDICTION OF MODAL PROPERTIES

Fundamental modal properties can be determined using the following equations that are suitable for manual calculations, finite element analysis, or other rational methods.

For typical rectangular floor bays with approximately uniformly distributed mass, the fundamental natural frequency, f_n, can be computed using the following equation. Its predictions are accurate according to Pabian et al. (2013),

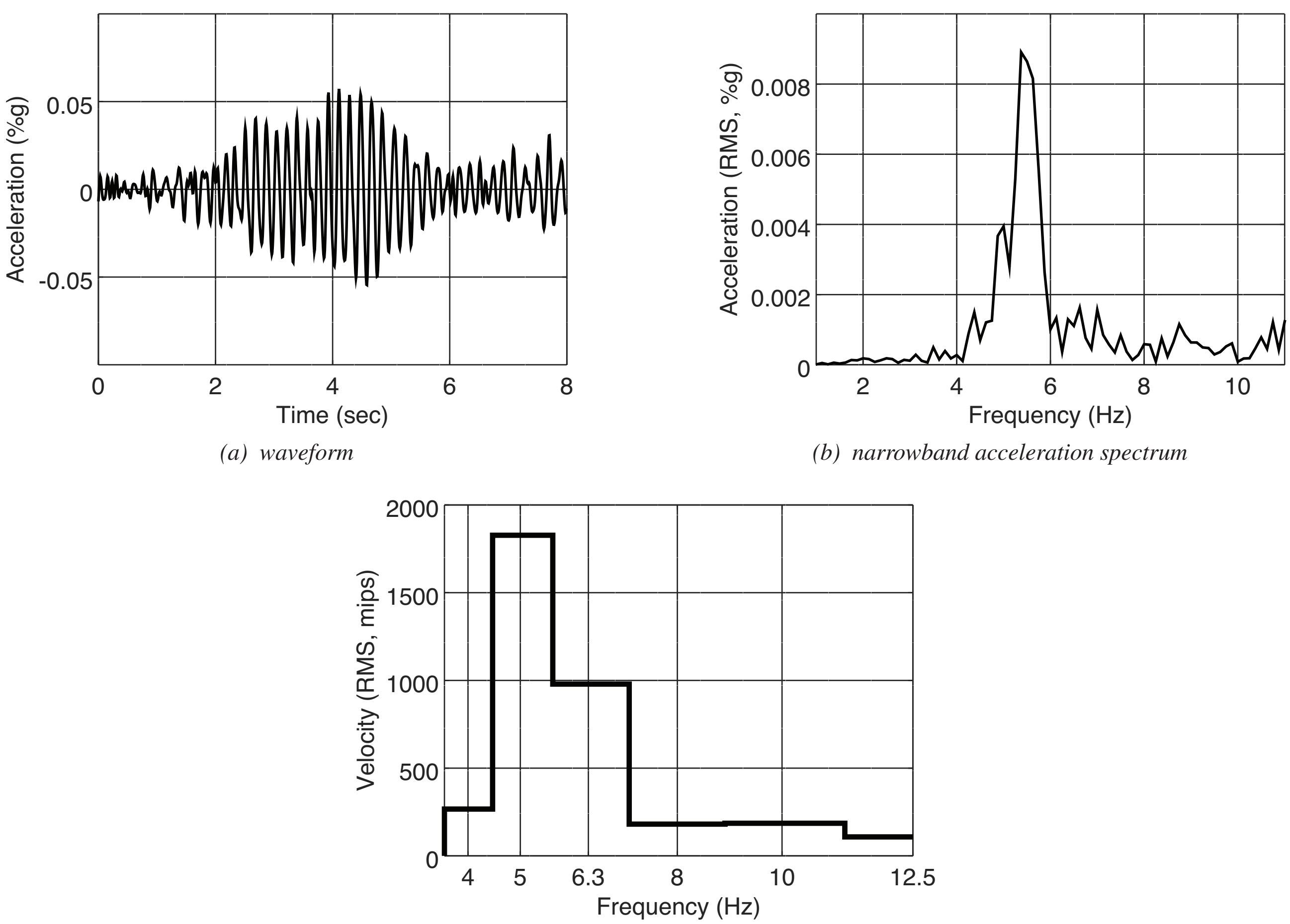

(a) waveform

(b) narrowband acceleration spectrum

(c) one-third octave velocity spectrum

Fig. 1. Example measured vibration due to walking.

and it is similar to the equation in the British Steel Construction Institute's P354 publication (Smith et al., 2009).

$$f_n = \min(f_b, f_g) \tag{1}$$

where f_b and f_g are the beam and girder natural frequencies from AISC Design Guide 11, Chapter 3.

The effective weight, W, of the fundamental mode can be computed using the following equation from AISC Design Guide 11 Chapter 4. W is double the weight of the effective mass, M_{eff} for load and acceleration at mid-bay (Allen and Murray, 1993).

$$W = \frac{\Delta_b}{\Delta_b + \Delta_g} W_b + \frac{\Delta_g}{\Delta_b + \Delta_g} W_g \tag{2}$$

where

Δ_b, Δ_g = beam and girder mode deflections (AISC Design Guide 11, Chapter 3)

W_b, W_g = beam and girder mode effective weights (AISC Design Guide 11, Chapter 4)

Often, the equipment or walker (or both) is away from mid-bay. This is considered in the Response Prediction section by scaling the mid-bay response by the ratio of the mode shape values.

For typical rectangular bays, the mode shape can be estimated as follows. If the beam natural frequency is lower than the girder natural frequency, then the mode shape is assumed to be the beam bending mode shown in Figure 2. In this assumed shape, the beam deflection is in a half sine wave pattern, with a maximum value of 1.0 at mid-bay. Perpendicular to the beams, the mode shape is assumed to be a half sine wave that extends to the edges of the adjacent bays. If the girder natural frequency is lower than the beam natural frequency, the mode shape is assumed to be a girder bending mode, which is similar to Figure 2 except that the half-sine wave parallel to the girders has a length of L_g. Equation 3 can be used to compute the mode shape value, ϕ, at the equipment or walker location. The equations can be adjusted for other boundary conditions or framing arrangements (e.g., significantly different girder lengths), based on engineering judgment.

Alternatively, the natural frequencies and mode shapes can be predicted using finite element analysis per AISC Design Guide 11, Chapter 7.

The viscous damping ratio, β, is estimated using AISC Design Guide 11, Chapter 4. The damping ratio varies from approximately 0.02 for laboratory floors with ceiling below but no partitions to 0.05 for floor bays with significant full-height partitions. It should be noted that the suggested damping ratios may differ considerably from the actual ones. Because the predicted response depends on β, there is considerable uncertainty in the prediction.

$$\phi = \sin\frac{\pi x}{L_b}\sin\frac{\pi(y + L_g)}{3L_g} \quad \text{if } f_b \le f_g \tag{3a}$$

$$\phi = \sin\frac{\pi(x + L_b)}{3L_b}\sin\frac{\pi y}{L_g} \quad \text{if } f_b > f_g \tag{3b}$$

FORCES DUE TO WALKING

For sensitive equipment evaluations, AISC Design Guide 11 defines four walking speeds: very slow, slow, moderate, and fast. Very slow walking applies in areas with short walking paths, such as a medical imaging control room or a small laboratory. For this category, the walking path is too short for a series of nearly identical footsteps that might cause a resonant buildup. Fast walking applies in areas, such as corridors, that do not limit the speed of walking. Slow and moderate walking are intermediate categories that can be used based on judgment. Table 1 indicates the step frequencies for these categories. The minimum frequency of slow walking, 1.5 Hz, is near the lower end of regular step frequencies listed in AISC Design Guide 11, Chapter 1. Similarly, the maximum frequency of fast walking is at the higher end of regular step frequencies, 2.2 Hz. The boundaries between slow and moderate walking, and moderate and fast walking, are approximately at the one-third points between 1.5 Hz and 2.2 Hz.

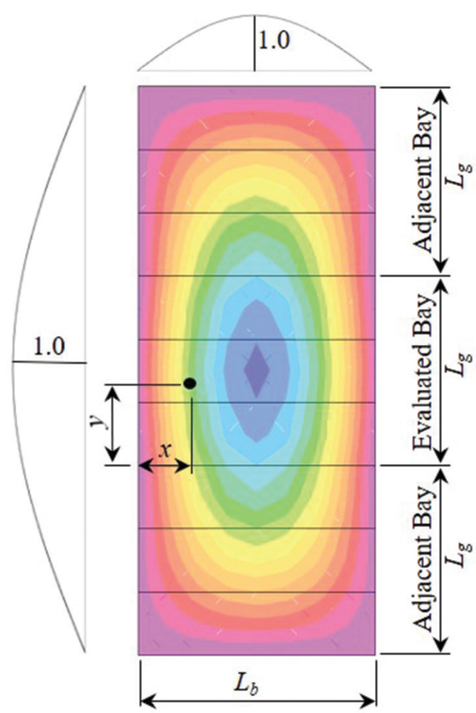

Fig. 2. Beam bending mode shape.

Table 1. Step Frequencies		
Category	**Range (Hz)**	**Mid-Range (Hz)**
Very slow	1.0–1.5	1.25
Slow	1.5–1.7	1.60
Moderate	1.7–2.0	1.85
Fast	2.0–2.2	2.10

Forces due to walking have been measured by various researchers. The measurements by Rainer et al. (1988) and Kerr (1998) have been influential in North American (Murray et al., 1997; Murray et al., 2016; NRCC, 2010) and European (Willford and Young, 2006; Smith et al., 2009) design guides. The footstep forces used for sensitive equipment in AISC Design Guide 11 are based on the database of more than 800 measurements by Kerr and others, reported in Willford et al. (2007a; 2007b).

Fourier Series

For the purpose of computing resonant responses due to walking, the walking force, $F(t)$, is represented by the following Fourier series limited to four harmonics.

$$F(t) = \sum_{i=1}^{4} \alpha_i Q \sin\left(2\pi i f_{step} t - \phi_i\right) \tag{4}$$

where

Q = reference bodyweight, lb

f_{step} = step frequency, Hz

t = time, sec

α_i = dynamic coefficient of the ith harmonic

ϕ_i = phase lag of the ith harmonic

The reference bodyweight is 168 lb to be consistent with Willford and Young (2006) and Smith et al. (2009), which use dynamic coefficients similar to those used herein.

The phase lag has extremely high variability. Zivanovic et al. (2007) indicated that measured phase lags varied uniformly from $-\pi$ to π. In the formulations described herein, the phase lag is not required.

Willford et al. (2007a) provided a good summary of dynamic coefficients (called "dynamic load factors" in their paper) measured by several researchers, including Kerr (1998). They plotted the dynamic coefficients for the first four harmonics versus frequency. The plots indicate: (1) the dynamic coefficients vary widely; (2) dynamic coefficients decrease slightly with increasing harmonic number; and (3) for a given harmonic, the dynamic coefficient increases slightly with increasing step frequency. The approximate average dynamic coefficients for the first four harmonics are 0.4, 0.07, 0.06, and 0.05.

The second through fourth harmonic dynamic coefficients at mid-range harmonic frequencies—product of mid-range step frequency from Table 1 and harmonic number—were curve-fit for slow, moderate, and fast walking to facilitate the development of resonant response prediction equations. The curve-fit for slow walking, for example, is in Figure 3. The resulting equation is:

$$\alpha = 0.0985e^{-\gamma f} \tag{5}$$

where

f = frequency, Hz

γ = 0.1, 0.09, and 0.08 for slow, moderate, and fast walking, respectively

Effective Impulse

From basic mechanics, the peak velocity of a mass, M, immediately after an impulse, I, is:

$$v_p = \frac{I}{M} \tag{6}$$

This relationship can be used to compute the peak velocity immediately after a footstep. The walking force is expressed as an effective impulse, I_{eff} in lb-sec, and the mass is the effective mass of the floor bay, M_{eff}, in lb-sec^2/in.

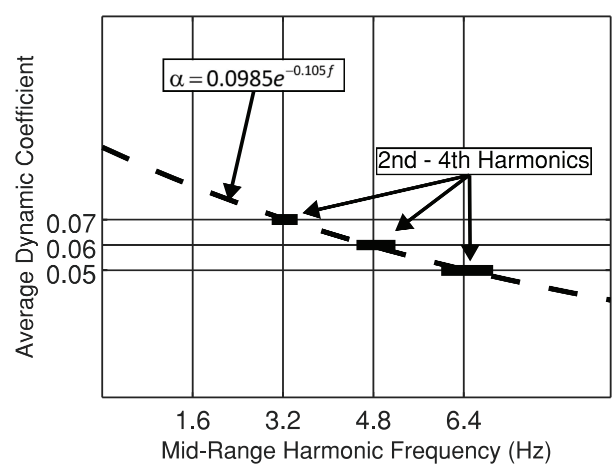

Fig. 3. Example curve-fit of dynamic coefficients.

The following effective impulse was adapted from Young and Willford (2001). They computed peak velocities of analytical representations of floors subjected to 880 measured footstep forces from Kerr (1998). [More information is found in Liu and Davis (2015).] For each case, the effective impulse was the product of the peak velocity and mass. The results indicated that the effective impulse increases as the step frequency increases and decreases as the natural frequency increases. The average effective impulse from their study is:

$$I_{eff} = \frac{f_{step}^{1.43}}{f_n^{1.30}} \frac{Q}{17.8} \tag{7}$$

where f_{step} is the step frequency. For the research described herein, f_{step} is the mid-range frequency from Table 1.

PREDICTION OF RESONANT RESPONSES

According to Rainer et al. (1988), only the "first three or four harmonics comprise the main dynamic components of walking forces." Thus, resonant responses are possible if the natural frequency does not exceed the maximum frequency of the fourth harmonic, which is called f_{4max} in AISC Design Guide 11. For slow walking, the maximum step frequency from Table 1 is 1.7 Hz, so f_{4max} = (1.7 Hz)(4) = 6.8 Hz. Similarly, for moderate and fast walking, respectively, f_{4max} is 8.0 Hz and 8.8 Hz.

Figure 4 is an example resonant response of a floor with a natural frequency of 5.18 Hz, due to walking at 5.18 Hz/3 = 1.73 Hz. The waveform indicates a resonant buildup followed by a short duration of sinusoidal vibration with nearly constant amplitude. According to research by the writers and their colleagues, the average number of footsteps in a resonant buildup is approximately six.

Figure 4(b) indicates very low responses to the first and second harmonics (1.73 Hz and 3.46 Hz) and that the vast majority of the response is due to the third harmonic, which is at the natural frequency—5.18 Hz in this example. Thus, the bay can be idealized as a single degree-of-freedom (SDOF) system with the natural frequency, effective mass, and damping of the bay, subjected to the harmonic force causing resonance. Figure 5 is the computed response to the harmonic, with frequency equaling the natural frequency and a 3-sec resonant buildup, followed by viscous decay.

Peak Acceleration and Velocity Due to Resonant Response

Using an SDOF idealization, the predicted peak acceleration, a_p, is the product of a calibration factor, R, steady-state acceleration, $a_{SteadyState}$, due to the harmonic force at the natural frequency, and resonant buildup factor, ρ (Liu, 2015), as shown in Equation 8. The steady-state acceleration and resonant buildup factor are computed using classical equations for an SDOF system subjected to a sinusoidal load at resonance (Chopra, 2011; Clough and Penzien, 1993).

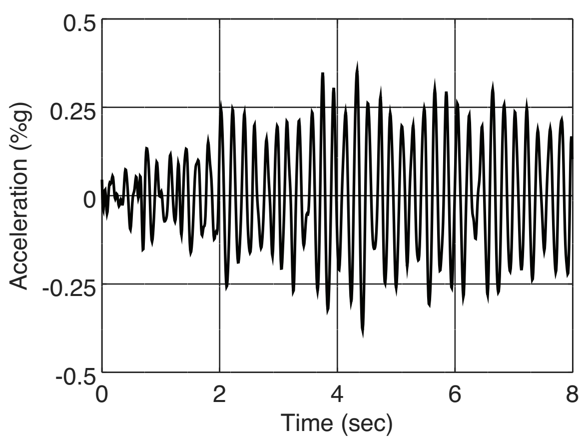

(a) waveform

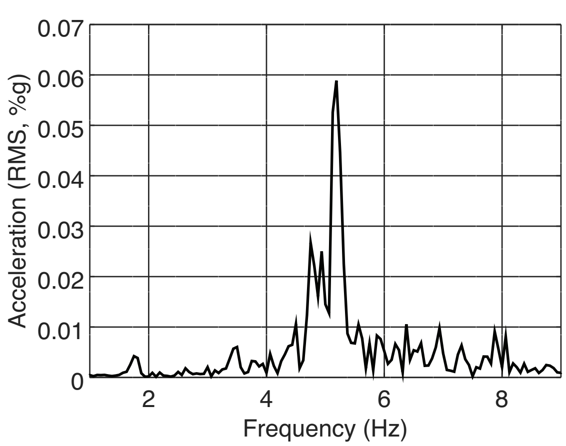

(b) narrowband spectrum

Fig. 4. Example measured resonant response.

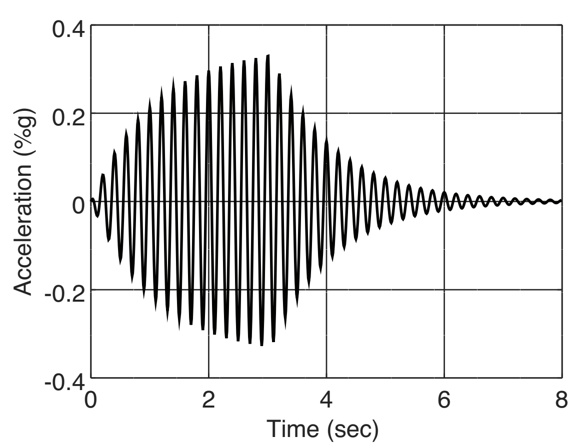

Fig. 5. Example computed response to the harmonic causing resonance.

$$a_p = Ra_{SteadyState} \tag{8}$$
$$= R\frac{\alpha_h Q}{2\beta M_{eff}}\left(1-e^{-\beta 2\pi f_n T_{BU}}\right)$$

where

R = calibration factor

T_{BU} = duration of resonant buildup, sec

α_h = average dynamic coefficient of the harmonic causing resonance

The effective mass of the fundamental mode, M_{eff}, is half the mass of the effective weight, W, from AISC Design Guide 11, Chapter 4 (Murray et al., 1997). Note that this effective mass applies when the load and acceleration are at mid-bay.

Liu (2015) compared predictions from Equation 8, with R = 1.0, with 65 measurements to determine the accuracy and establish the calibration factor. The predictions were slightly conservative with an average measured-to-predicted ratio of 0.870 and a coefficient of variation (COV) of 33%. An R value of 1.3 results in 10% of measured accelerations exceeding predicted accelerations.

Equation 8 was simplified for design guide implementation as follows. The damping ratio is usually between 0.03 and 0.05. The average resonant buildup is due to approximately six footsteps, so the resonant buildup duration, T_{BU}, ranges from 6/2.2 Hz = 2.7 sec to 6/1.6 Hz = 3.8 sec. For these values of β and T_{BU}, and $f_n \geq 6$ Hz, the resonant buildup factor, ρ, is between 0.95 and 1.0, so it is conservatively taken as 1.0.

After setting R equal to 1.3, substituting Equation 5 for α_h, setting ρ equal to 1.0 and simplifying, the peak acceleration due to a resonant buildup is:

$$a_p = \frac{21.5}{\beta W}e^{-\gamma f_n}g \tag{9}$$

where g is the gravitational acceleration and the other variables are defined previously.

Figure 6 summarizes the measured-to-predicted ratio for the measurements by Liu (2015) and predictions from Equation 9.

The peak velocity is approximately equal to the peak acceleration divided by $2\pi f_n$. In units of mips, the peak velocity due to a resonant buildup is:

$$V_p = \frac{1.32\times 10^9}{\beta W f_n}e^{-\gamma f_n} \tag{10}$$

Maximum Narrowband Acceleration and Velocity Due to a Resonant Response

The maximum narrowband spectral acceleration, shown as the highest peak in Figure 1(b), is computed by Fourier transformation of the waveform in Figure 5. The peak acceleration in the waveform is from Equation 8 with the calibration factor removed.

The resonant buildup is assumed to be 3 sec long, which is approximately the average duration considering six footsteps at the average step frequency of 2 Hz. The remainder of the waveform is viscous decay. The duration of the waveform has a significant influence on the computed spectral acceleration. Shorter durations result in higher spectral accelerations because a larger portion of the waveform consists of the buildup, which has higher responses than the decay portion. The shortest reasonable duration that is expected to be used by site surveyors is 8.0 sec because this results in a 0.125-Hz frequency resolution. Shorter durations result in spectra that are overly coarse. Thus, 8 sec is used herein.

The Fourier transformation results in the following equation for the maximum magnitude. See Liu (2015) for a detailed derivation. Note that the result is an RMS acceleration.

$$A_{NB} = R\frac{27}{\sqrt{2}}\frac{\alpha_h}{\beta^2 W f_n T}\left[C-\left(1-e^{-C}\right)\left(e^{-C}\right)^{r_t}\right]g \tag{11}$$

where

T = total duration of waveform, sec

r_t = duration of decay divided by duration of buildup

The variable, C, is:

$$C = 12\pi\beta H \tag{12}$$

where H is the number of the harmonic that causes resonance, estimated by:

$$H = f_n / f_{step} \tag{13}$$

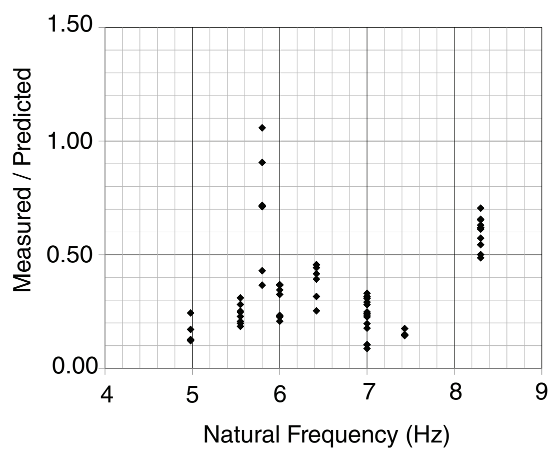

Fig. 6. Comparisons of measurements and predictions, resonant responses, peak acceleration.

Table 2. One-Third Octave Bands		
Lower Limit (Hz)	**Center Frequency (Hz)**	**Upper Limit (Hz)**
3.55	4.0	4.47
4.47	5.0	5.62
5.62	6.3	7.08
7.08	8.0	8.91
8.91	10.0	11.2
11.2	12.5	14.1
14.1	16.0	17.8
17.8	20.0	22.4

The step frequency, f_{step} is the mid-range frequency from Table 1.

For the database of floors mentioned previously, the average measured-to-predicted ratio, with $R = 1.0$, was 0.780 and the COV was 46.2%. The calibration factor, R, for a 10% probability of exceedance, is 1.3 (Liu, 2015).

Equation 11 was simplified for design guide implementation as follows. The second term was omitted because it is much smaller than C. After substituting Equation 5 for α_h, including $R = 1.3$, and simplifying, the narrowband spectral acceleration maximum RMS magnitude is:

$$A_{NB} = \frac{7.2}{\beta W} e^{-\gamma f_n} g \tag{14}$$

Figure 7 summarizes the measured-to-predicted ratio for the aforementioned measurements and predictions from Equation 14.

The narrowband spectral velocity equals the spectral acceleration divided by $2\pi f$ for all frequencies, f. After simplifying, the narrowband spectral velocity maximum magnitude—in mips, RMS—due to a resonant buildup is:

$$V_{NB} = \frac{442 \times 10^6}{\beta W f_n} e^{-\gamma f_n} \tag{15}$$

Maximum One-Third Octave Acceleration and Velocity Due to a Resonant Response

The one-third octave velocity is determined by bandwidth conversion from narrow bands to the bands summarized in Table 2. A one-third octave band encompasses many narrow bands, exemplified by the band with 5 Hz center frequency in Figure 8, so it contains the summation of the energies of the spectral accelerations in the contained narrow bands.

The energy of the signal at a narrowband frequency, f, is:

$$E_{NB}(f) = A_{NB,R=1}(f)^2 \tag{16}$$

where $A_{NB,R=1}$ is the peak acceleration from Equation 11 with $R = 1.0$.

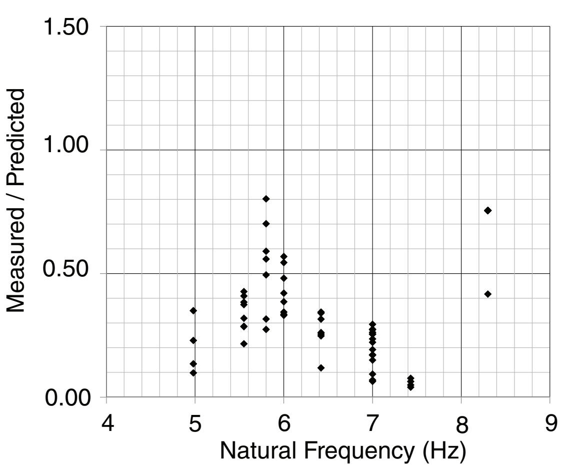

Fig. 7. Comparisons of measurements and predictions, resonant responses, narrowband acceleration.

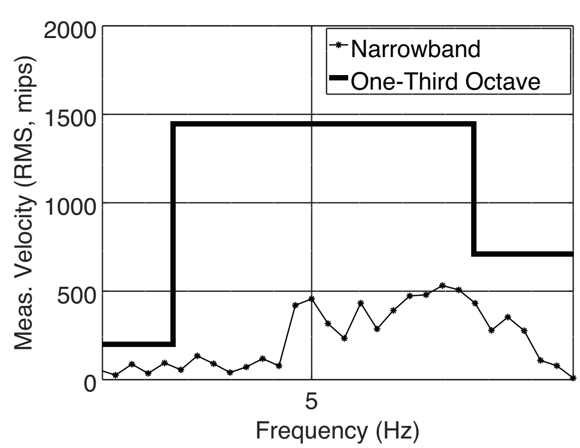

Fig. 8. Example one-third octave band.

The energy spectral density (ESD) at frequency, f, is:

$$ESD(f) = A_{NB,R=1}(f)^2/\Delta f \tag{17}$$

where the narrowband spectral resolution, Δf, is the reciprocal of the duration, T, of the walking event used to compute the narrowband spectrum.

The energy of the signal within a one-third octave band is the area under the ESD curve in the one-third octave band (Liu, 2015). Typically, one peak in the narrowband spectrum [Figure 1(b)] fits within a one-third octave band. This peak can be idealized as a triangle with maximum magnitude equal to the value from Equation 11 with R = 1.0. The width of the triangle is approximately 10% of the harmonic frequency (Brownjohn et al., 2004), which equals the natural frequency. The energy spectral density of this peak is slightly curved as shown in the example in Figure 9. In this example, the natural frequency is 6.2 Hz, so the peak is 0.62 Hz wide. This peak fits inside the 6.3-Hz one-third octave band, which has lower and upper bounds shown dashed on the plot.

The energy of the signal within the one-third octave band is:

$$E_{1/3} = \int ESD(f)\,df = \frac{1}{3}\frac{(A_{NB,R=1})^2}{\Delta f}\frac{f_n}{10} = \frac{(A_{NB,R=1})^2 T f_n}{30} \tag{18}$$

where

$A_{NB,R=1}$ = spectral acceleration magnitude from Equation 11 with R = 1.0

T = duration of waveform used in the Fourier transformation, 8.0 sec

Using Equations 16 and 18, the uncalibrated one-third octave acceleration is derived as follows. (The uncalibrated version is carried through this calculation because the calibration factor is potentially different for narrowband acceleration and one-third octave acceleration.)

$$\begin{aligned} E_{1/3} &= A_{1/3,R=1}^2 \\ \frac{(A_{NB,R=1})^2 T f_n}{30} &= A_{1/3,R=1}^2 \\ A_{1/3,R=1} &= A_{NB,R=1}\sqrt{\frac{T f_n}{30}} \end{aligned} \tag{19}$$

The one-third octave velocity is the acceleration divided by $2\pi f_n$:

$$V_{1/3,R=1} = \frac{A_{NB,R=1}}{2\pi f_n}\sqrt{\frac{T f_n}{30}} = \frac{A_{NB,R=1}}{2\pi}\sqrt{\frac{T}{30 f_n}} \tag{20}$$

For the database of floors mentioned above, the average measured-to-predicted velocity ratio was 0.640 and the COV was 38.7%. The calibration factor, R, for a 10% probability of exceedance, is 1.0 (Liu, 2015).

Equations 19 and 20 are simplified for design guide implementation by substituting Equation 14 with R = 1.0 for $A_{NB,R=1}$ and using T = 8 sec. After simplification, the one-third octave acceleration, RMS, due to a resonant buildup, is:

$$A_{1/3} = \frac{6.39}{\beta W} e^{-\gamma f_n} g \tag{21}$$

Also, the one-third octave velocity, RMS in mips, is:

$$V_{1/3} = \frac{175\times 10^6}{\beta W \sqrt{f_n}} e^{-\gamma f_n} \tag{22}$$

Figure 10 summarizes the measured-to-predicted ratio for the measurements mentioned above and predictions from Equation 22.

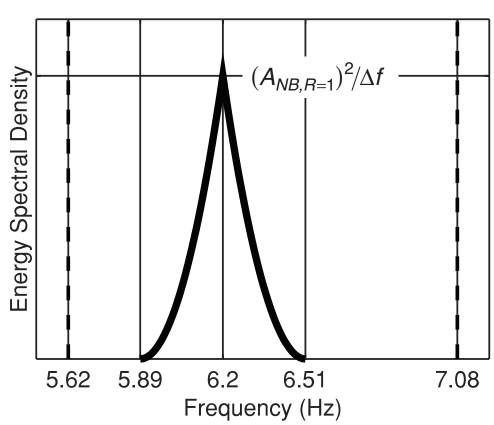

Fig. 9. Energy spectral density.

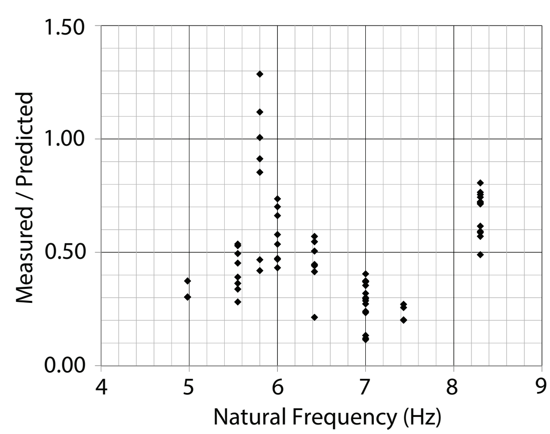

Fig. 10. Comparisons of measurements and predictions, resonant responses, one-third octave velocity.

PREDICTION OF IMPULSE RESPONSES

If the fundamental frequency exceeds the maximum frequency of the fourth harmonic, f_{4max}, resonance will not occur, and the maximum response resembles a series of individual impulse responses with little or no buildup. An example measured waveform is shown in Figure 11. The higher responses near the middle of the waveform are due to footsteps near mid-bay. The development in the following is described in detail in Liu (2015) and Liu and Davis (2015).

Peak Acceleration and Velocity Due to Impulse Response

The peak velocity immediately after a footstep is the product of a calibration factor, R, and the effective impulse from Equation 7, divided by the effective mass of the bay. Multiple modes contribute significantly to impulse responses, so a factor, $R_M = 2.0$, from Liu and Davis (2015), is included.

$$v_p = RR_M \frac{I_{eff}}{M_{eff}} \tag{23}$$

$$= RR_M \frac{Q}{17.8} \frac{f_{step}^{1.43}}{f_n^{1.30}} \frac{2g}{W}$$

The peak acceleration is approximately equal to the peak velocity multiplied by $2\pi f_n$:

$$a_p = RR_M \frac{Q}{17.8} \frac{f_{step}^{1.43}}{f_n^{1.30}} \frac{2g}{W} (2\pi f_n) \tag{24}$$

A total of 89 measured peak accelerations were compared to predictions from Equation 24, with R = 1.0, to assess the accuracy of the equation and establish the calibration factor. The average measured-to-predicted ratio was 0.966 and the COV was 26%. R = 1.3 results in 10% of measured accelerations exceeding predicted accelerations (Liu, 2015; Liu and Davis, 2015).

After simplification, the following two equations are recommended. Note that v_p is in units of mips.

$$v_p = \frac{18.9 \times 10^9}{W} \frac{f_{step}^{1.43}}{f_n^{1.30}} \tag{25}$$

$$a_p = \frac{308}{W} \frac{f_{step}^{1.43}}{f_n^{0.3}} g \tag{26}$$

where f_{step} is the mid-range frequency from Table 1.

Figure 12 summarizes the measured-to-predicted ratio for the measurements mentioned above and predictions from Equation 26.

Maximum Narrowband Acceleration and Velocity Due to a Series of Impulse Responses

The maximum narrowband acceleration due to a series of impulses responses is computed by Fourier transforming the idealized waveform in Figure 13 and then adjusting for several differences between the idealized waveform and measured waveforms.

The peak acceleration in the idealized waveform is from Equation 26 with the calibration factor, 1.3, removed. This peak acceleration is for acceleration at mid-bay due to a footstep at mid-bay. The remainder of the response to each footstep is viscous decay. Identical footsteps are appended at the step frequency, so the waveform is perfectly periodic. The Fourier transformation results in a very complicated equation for the spectral peak at each harmonic of the walking force (Liu and Davis, 2015). The maximum spectral magnitude (peak, not RMS) for this idealized walking event, $A_{NB,I}$, at the natural frequency, is:

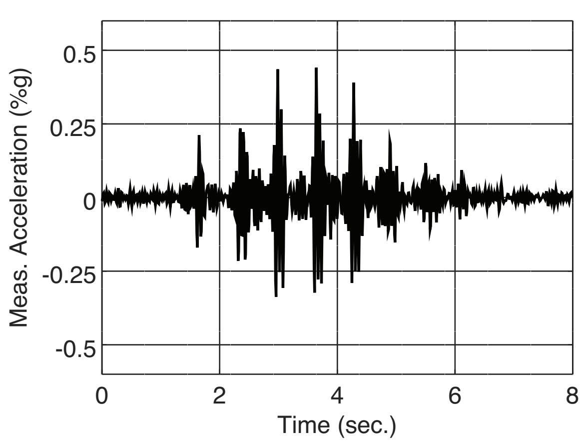

Fig. 11. Example series of impulse responses.

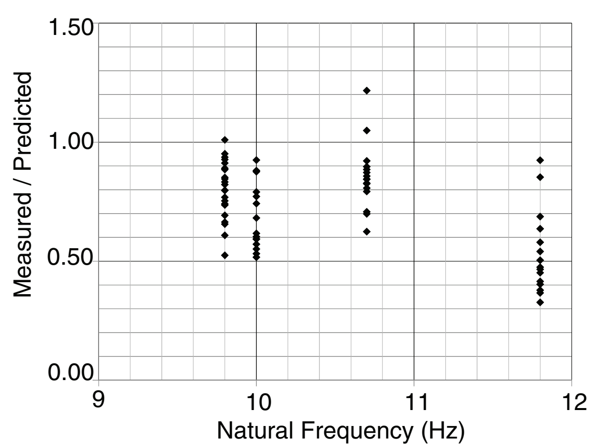

Fig. 12. Comparisons of measurements and predictions, impulse responses, peak acceleration.

$$A_{NB,I} = a_{p,R=1} \frac{1 - e^{-2\pi\beta H}}{2\pi\beta H} \tag{27}$$

where $a_{p,R=1}$ is from Equation 24 with R = 1.0, and H is the number of the harmonic at the natural frequency.

Actual footsteps are not identical, nor are they repeated precisely at the step frequency. This results in energy being leaked into frequencies adjacent to each harmonic frequency, and lower spectral peaks. This is considered with the imperfect footsteps reduction factor, $R_I = 0.6$, which is based on research by Brownjohn et al. (2004).

Actual walking events do not have infinite durations as used in the Fourier transformation leading to Equation 27. Recall that the objective is to predict what the site surveyor will measure, and it is assumed that the Fourier transformations will be of waveforms lasting 8 sec. The duration of the series of impulse responses varies, but is taken as 4 sec, see Figure 11 for an example. This results in a duration adjustment factor, $R_D = 0.5$.

Actual walking events do not have each footstep at mid-bay. Instead, some footsteps will be applied near mid-bay where the mode shape values are maximal and others will be applied away from mid-bay. For walking that traverses an entire bay with a half sine wave mode shape, the adjustment factor is 0.7. Slightly conservatively, the adjustment factor, R_L, is taken as 0.9.

After these adjustments are made and a calibration factor, R, is added, the maximum RMS magnitude is:

$$A_{NB} = \frac{1}{\sqrt{2}} R R_I R_D R_L a_{p,R=1} \frac{1 - e^{-2\pi\beta H}}{2\pi\beta H} \tag{28}$$

where $a_{p,R=1}$ is from Equation 24 with R = 1.0, and H is the number of the harmonic at the natural frequency.

Measurements from the database mentioned above were compared to predictions from Equation 28 with R = 1.0 to assess the accuracy of the equation and establish the calibration factor. The average measured-to-predicted ratio was 0.790 and the COV was 32%. An R value of 1.1 results in 10% of measured accelerations exceeding predicted accelerations (Liu, 2015; Liu and Davis, 2015).

After the inclusion of the calibration factor and simplification, the RMS magnitude is:

$$A_{NB} = \frac{7.93}{\beta W} \frac{f_{step}^{2.43}}{f_n^{1.3}} \left(1 - e^{-2\pi\beta f_n / f_{step}}\right) g \tag{29}$$

Figure 14 summarizes the measured-to-predicted ratio for the aforementioned measurements and predictions from Equation 29.

The narrowband velocity magnitude is computed by dividing Equation 29 by $2\pi f_n$. The RMS magnitude in mips is:

$$V_{NB} = \frac{487 \times 10^6}{\beta W} \frac{f_{step}^{2.43}}{f_n^{2.3}} \left(1 - e^{-2\pi\beta f_n / f_{step}}\right) \tag{30}$$

Maximum One-Third Octave Acceleration and Velocity Due to a Series of Impulse Responses

The one-third octave acceleration and velocity due to a series of impulse responses were determined using the bandwidth conversion method described above for resonant responses.

The one-third octave velocity is computed using Equation 20 with $A_{NB,R=1}$ from Equation 28. Measurements from the database mentioned above were compared to predictions to assess the accuracy of the predictions and establish the calibration factor. The average measured-to-predicted ratio was 0.736 and the COV was 34%. An R value of 1.1 results in 10% of measured accelerations exceeding predictions (Liu, 2015; Liu and Davis, 2015).

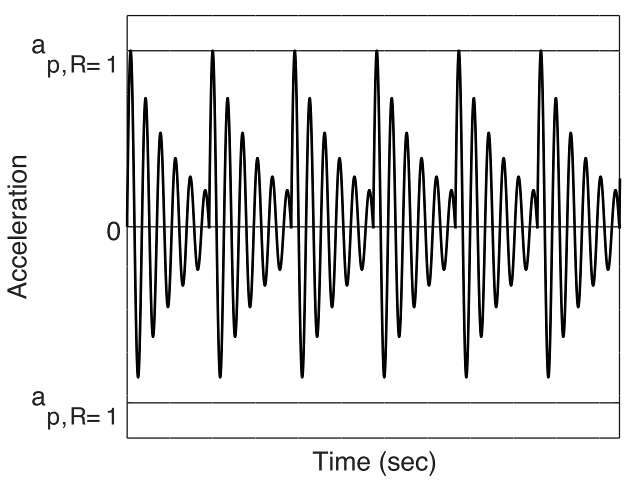

Fig. 13. Idealized impulse series of impulse responses.

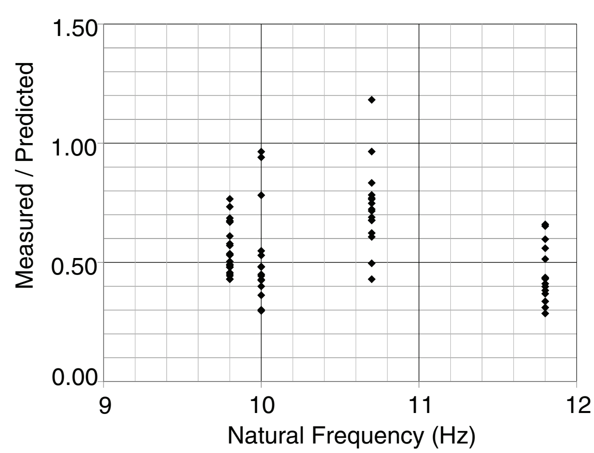

Fig. 14. Comparisons of measurements and predictions, impulse responses, narrowband acceleration.

Table 3. Boundaries of Intermediate Zones		
Walking Speed	**f_L (Hz)**	**f_U (Hz)**
Slow	6.0	8.0
Moderate	7.0	9.0
Fast	8.0	10.0

After including the calibration factor and simplifying, the one-third octave RMS velocity due to a series of impulse responses in mips is:

$$V_{1/3} = \frac{252\times10^6}{\beta W}\frac{f_{step}^{2.43}}{f_n^{1.8}}\left(1-e^{-2\pi\beta f_n/f_{step}}\right) \tag{31}$$

Figure 15 summarizes the measured-to-predicted ratio for the aforementioned measurements and predictions from Equation 31.

The one-third octave acceleration is computed using Equation 19 with $A_{NB,R=1}$ from Equation 28. After including the calibration factor of R = 1.1 and simplifying, the RMS acceleration is:

$$A_{1/3} = \frac{4.2}{\beta W}\frac{f_{step}^{2.43}}{f_n^{0.8}}\left(1-e^{-2\pi\beta f_n/f_{step}}\right)g \tag{32}$$

RESPONSE PREDICTION

The first step in predicting the response is the selection of the tolerance limit. The form (peak acceleration) of the response prediction must obviously match the tolerance limit.

As explained in the Resonant Response section, resonant responses are possible when the natural frequency does not exceed the maximum frequency of the fourth harmonic, f_{4max}. Impulse responses are possible for any natural frequency. The controlling response is the maximum of the two, and when a resonant response is possible, it usually greatly exceeds the impulse response. This is illustrated in Figure 16. This example is for slow walking (f_{4max} = 6.8 Hz) on a floor with W = 250 kips and β = 0.05. As f_n crosses f_{4max} on the plot, the controlling velocity decreases abruptly by a large amount, which would not occur in reality. It is much more likely that the behavior would gradually change from resonant to impulse response as the natural frequency crosses f_{4max}, thus defining a region of intermediate responses. For design guide implementation, linear interpolation is used in this region, which is 2 Hz wide and approximately centered on f_{4max} as shown in Figure 16. The lower and upper bounds of the intermediate zones are in Table 3.

For very slow walking, the impulse response is computed regardless of the natural frequency. For slow, moderate, and fast walking, if the natural frequency does not exceed f_L, then the resonant response is computed using equations from the Resonant Responses section. If the natural frequency exceeds f_U, then the impulse response is computed using equations from the Impulse Responses section. If the natural frequency is between f_L and f_U, then the intermediate response is computed by linear interpolation between the resonant response at f_L and the impulse response at f_U. In equation form, using one-third octave velocity for example:

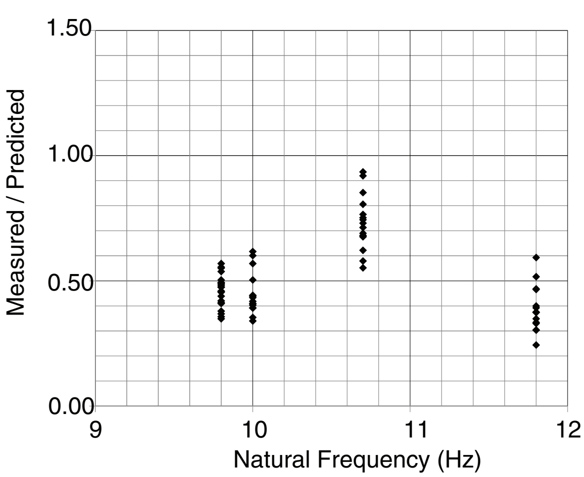

Fig. 15. Comparisons of measurements and predictions, impulse responses, one-third octave velocity.

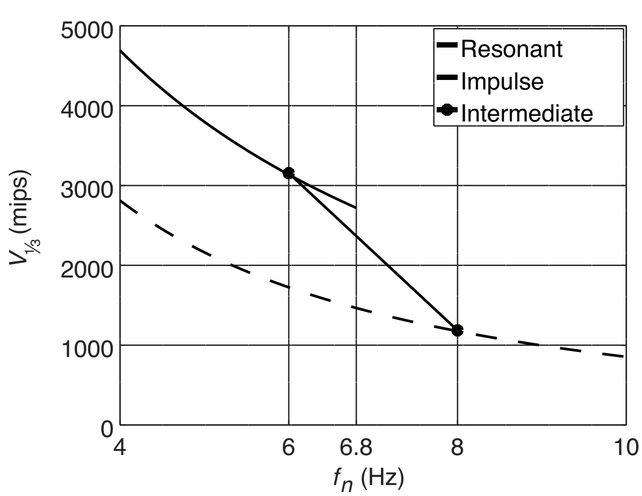

Fig. 16. Example velocity as a function of natural frequency.

$$V_{1/3} = \begin{vmatrix} \dfrac{175\times10^6}{\beta W\sqrt{f_n}} e^{-\gamma f_n} \\ \dfrac{252\text{x}10^6}{\beta W} \dfrac{f_{step}^{2.43}}{f_n^{1.8}} \left(1 - e^{-2\pi\beta f_n / f_{step}}\right) \end{vmatrix} \quad \text{if } f_n \le f_L \tag{33a}$$

$$V_{1/3} = \frac{252\times10^6}{\beta W} \frac{f_{step}^{2.43}}{f_n^{1.8}} \left(1 - e^{-2\pi\beta f_n / f_{step}}\right) \quad \text{if } f_n > f_U \tag{33b}$$

For one-third octave velocity, the resonant response controls if $f_n \le f_L$, so Equation 33a and 33b reduce to:

$$V_{1/3} = \begin{vmatrix} \dfrac{175\times10^6}{\beta W\sqrt{f_n}} e^{-\gamma f_n} \ \text{if } f_n \le f_L \\ \dfrac{252\times10^6}{\beta W} \dfrac{f_{step}^{2.43}}{f_n^{1.8}} \left(1 - e^{-2\pi\beta f_n / f_{step}}\right) \ \text{if } f_n > f_U \end{vmatrix} \tag{34}$$

All response equations presented above are for the worst-case scenario of mid-bay vibration response to walking through mid-bay. Very often, the equipment is located away from mid-bay. Also, walls and other obstacles often prevent walking through mid-bay. Tolerance limits are often very stringent, so the response should typically be computed based on the actual equipment location and walking path location. This is accomplished by scaling the mid-bay response by the ratio of mode shape values.

When the equipment is away from mid-bay and the walker can pass through mid-bay, the predicted response, using velocity for example, is:

$$V = V_{midbay} \frac{\phi_e}{\phi_{midbay}} \tag{35}$$

where

V = response at the equipment

V_{midbay} = response at mid-bay due to walking through mid-bay

ϕ_e = mode shape value at the equipment location

ϕ_{midbay} = mode shape value at mid-bay

When the walking path does not pass through mid-bay, and the equipment is at mid-bay, the predicted response is:

$$V = V_{midbay} \frac{\phi_w}{\phi_{midbay}} \tag{36}$$

where ϕ_w is the maximum mode shape value along the walking path.

When neither the equipment nor the walking path is at mid-bay, the predicted response is:

$$V = V_{midbay} \frac{\phi_e}{\phi_{midbay}} \frac{\phi_w}{\phi_{midbay}} \tag{37}$$

The mode shape values can be determined by any rational method such as finite element analysis per AISC Design Guide 11, Chapter 7. For simple cases with typical framing, Equation 3 can be used or adjusted for other boundary conditions.

COMMENTARY ON FIRST AND SECOND EDITIONS OF AISC DESIGN GUIDE 11, CHAPTER 6

The methods in the first and second editions of AISC Design Guide 11, Chapter 6, were derived using significantly different models, so the velocity predictions differ significantly in some cases. The following are the main differences between the two editions.

For frequencies above 8–9 Hz, the responses are impulsive, and the second edition takes this into account. Impulse responses are not strongly linked to natural frequency, but are strongly linked to mass. Thus, natural frequency often plays a less prominent role and mass plays a more prominent role in the second edition than in the first edition.

Response is not a function of damping in the first edition. However, in the second edition, most of the responses are functions of damping because the spectral responses depend on the entire waveform, including the decay portion. It is noted that this makes velocity comparisons difficult between the two editions.

In the first edition, moderate walking causes much higher velocities than those from slow walking. Similarly, fast walking causes much higher velocities than those from moderate walking. Our measurements indicate the differences are not as large as those in the first edition. Thus, the second edition responses for various speeds are much closer together. Also, the speed categories are different. Slow walking in the first edition is fairly close to very slow walking in the second edition.

CONCLUSIONS

Floor vibration tolerance limits for sensitive equipment, in terms of various acceleration and velocity measures, are much more stringent than those for human comfort.

The floor response to walking is affected by the speed of walking, natural frequency, effective mass, and damping. Walking in higher speed categories causes higher responses. Higher natural frequency, effective mass, and damping cause lower responses. For lower frequency floors, the highest response is due to a resonant buildup. For higher frequency floors, the highest response is due to a series of impulse responses to individual footsteps.

Fairly simple equations for resonant and impulse responses are recommended herein for design. These equations use natural frequency, effective weight, and damping estimates from AISC Design Guide 11; they are suitable for manual calculations. Note that natural frequency and effective mass or weight can be determined through other means such as finite element analyses. The response prediction equations have been experimentally verified with fairly large databases of walking measurements on lower and higher frequency floors.

Vibration of floors supporting sensitive equipment is usually very objective. Also, reduction of vibration levels of a constructed floor is difficult and expensive. Thus, each response prediction equation includes a calibration factor that results in predictions that exceed measured vibration levels 90% of the time.

ACKNOWLEDGMENTS

The authors thank AISC for funding the research that resulted in the methods described herein.

REFERENCES

Allen, D.E. and Murray, T.M. (1993), "Design Criteria for Vibrations Due to Walking," *Engineering Journal*, AISC, Vol. 30, No. 4, pp. 117–129.

Brownjohn, J.M.W., Pavic, A., and Omenzetter, P. (2004), "A Spectral Density Approach for Modelling Continuous Vertical Forces on Pedestrian Structures Due to Walking," *Canadian Journal of Civil Engineering*, Vol. 31, No. 1, pp. 65–77.

Chopra, A.K. (2011), *Dynamics of Structures: Theory and Applications to Earthquake Engineering*, 4th Ed., Prentice Hall, Upper Saddle River, N.J.

Clough, R.W. and Penzien, J. (1993), *Dynamics of Structures*, 2nd Ed., McGraw-Hill, New York, N.Y.

Kerr, S.C. (1998), "Human Induced Loading on Staircases," PhD Thesis, University of London, London, England.

Liu, D. (2015), "Vibration of Steel-Framed Floors Supporting Sensitive Equipment in Hospitals, Research Facilities, and Manufacturing Facilities," PhD Dissertation, University of Kentucky, Lexington, Ky. (in preparation).

Liu, D. and Davis, B. (2015), "Walking Vibration Response of High-Frequency Floors Supporting Sensitive Equipment," *Journal of Structural Engineering*, Vol. 141, No. 8.

Murray, T.M., Allen, D.E., and Unger, E.E. (1997), *Floor Vibrations Due to Human Activity*, Design Guide 11, AISC, Chicago, Ill.

Murray, T.M., Allen, D.E., Unger, E.E., and Davis, D.B. (2016), *Vibration of Steel-Framed Structural Systems Due to Human Activity*, Design Guide 11, 2nd Ed., AISC, Chicago, Ill.

NRCC (2010), *National Building Code of Canada*, National Research Council of Canada, Ottawa, Canada.

Pabian, S., Thomas, A., Davis, B., and Murray, T.M. (2013), "Investigation of Floor Vibration Evaluation Criteria Using an Extensive Database of Floors," *Proceedings of the ASCE/SEI Structures Congress*, ASCE, May 2–3, Pittsburgh, Pa., pp. 2,478–2,486.

Rainer, J.H., Pernica, G., and Allen, D.E. (1988), "Dynamic Loading and Response of Footbridges," *Canadian Journal of Civil Engineering*, Vol. 15, No. 1, pp. 66–71.

Smith, A.L., Hicks, S.J., and Devine, P.J. (2009), *Design of Floors for Vibration: A New Approach*, (Revised), SCI P354, The Steel Construction Institute (SCI), Silwood Park, Ascot, Berkshire.

Ungar, E.E. and White, R.W. (1979), "Footfall-Induced Vibrations of Floors Supporting Sensitive Equipment," *Sound and Vibration*, Vol. 13, October, pp. 10–13.

Ungar, E., Zapfe, J., and Kemp, J. (2006), "Predicting Footfall-Induced Floor Vibrations Relative to Criteria for Sensitive Apparatus," *Proceedings of the ASCE/SEI Structures Congress*, ASCE, May 18–21, St. Louis, Mo., pp. 1–13.

Willford, M. and Young, P. (2006), *A Design Guide for Footfall Induced Vibration of Structures*, CCIP-016, The Concrete Centre, Surrey, UK.

Willford, M., Young, P., and Field, C. (2007a), "Predicting Footfall-Induced Vibration: Part 1," *Structures and Buildings*, Vol. 160, No. SB2, pp. 65–72.

Willford, M., Young, P., and Field, C. (2007b), "Predicting Footfall-Induced Vibration: Part 2," *Structures and Buildings*, Vol. 160, No. SB2, pp. 73–79.

Young, P. and Willford, M. (2001), *Towards a Consistent Approach to the Prediction of Footfall-Induced Structural Vibration,* Internal Document, Ove Arup and Partners, London, UK.

Zivanovic, S., Pavic, A., and Reynolds, P. (2007), "Probability-Based Prediction of Multi-Mode Vibration Response to Walking Excitation," *Engineering Structures*, Vol. 29, No. 6, pp. 942–954.